27th Summer School and International Symposium on the Physics of Ionized Gases (SPIG 2014) IOP Publishing
Journal of Physics: Conference Series **565** (2014) 012016 doi:10.1088/1742-6596/565/1/012016

Measurements and models of transient and stationary regimes of glow discharge in argon

M N Stankov
Department of Physics, Faculty of Science and Mathematics, University of Niš, Višegraska 33, PO box 224, 18001 Niš, Serbia

E-mail: marjansstankov@gmail.com

Abstract. The experimental and theoretical analyses of different regimes of argon DC glow discharge are reported. The experiments were carried out on the argon gas tube with a plane-parallel electrode system made from OFHC (oxygen-free high thermal conductivity) copper. Modelling of the static breakdown voltages was performed by simple fluid model. The applicability of fluid models for modelling of $I-U$ (current-voltage) characteristics at different values of pd (pressure times inter-electrode distance) is tested. The formative time delays are determined from experiment and compared to modeled values obtained by [1D] and [2D] fluid models. The memory curve $\overline{t_d}(\tau)$ (the dependence of the mean value of breakdown time delay on the relaxation time) is presented and the main processes responsible for the memory effect were determined by applying the analytical and numerical models.

1. Introduction

The application of all types of gas discharges in various fields of technology is very common, like for plasma etching, deposition and implantation of thin films, surfaces cleaning from the oxides, metallic and organic contaminants, laser and light sources technology, gas switches development, medical treatment, etc [1-7]. Beside the experimental research, different analytical and numerical models are used very commonly for better understanding of physical processes in various types of gas discharges. Numerical models used for glow discharge modelling can be classified as fluid, particles and hybrid models. Numerical modelling by computer was used for the first time for discharge simulation in 1958 [8] and after that its applicability has rapidly increased [9-12]. The investigation of breakdown time delays is also very useful for the analysis of glow discharges. The information about kinetics of atomic and molecular species remaining from the preceding glow and reactions rate coefficients may be estimated by the analysis of memory curve (the dependence of the mean value of breakdown time delay on the relaxation time $t_d(\tau)$).Memory effect in inert (argon) and molecular gases (nitrogen) was explained by long lived metastable states remaining from the preceding glow [13, 14]. However, the effective lifetimes of metastable states are very short due to quenching and memory effect was explained by the process of surface recombination of nitrogen atoms on the tube walls, while secondary electrons initiating breakdown are produced on the cathode surface [15-17].

The results of measurements and modelling are presented in this report. The theoretical description of different fluid models is presented in section 2, while the details of the experiment are given in section 3. In section 4, Paschen curve modelling is performed by simple fluid model and results are compared to experimental data. The applicability of different fluid models for *I-U* characteristics

modelling is analysed in section 5. The different analytical and numerical models are applied for the modelling of formative time delays and results are presented in section 6. The analysis of memory curve is given in section 7 and finally, short conclusion is presented in section 8.

2. Different fluid models

Different fluid models are often used for glow discharge modelling and the most common are simple and extend fluid models [18-20]. In the simple fluid model electron transport and kinetic coefficients are the function of reduced field [19], while in the extended fluid model these coefficients are the function of mean electron energy [20]**.** Although the fluid model with nonlocal ionization agrees very well with experiments and hybrid models [21], it is used less frequently than the previous mentioned models.

The simple fluid model consists of continuity equation and Poisson's equation:

$$\frac{\partial n^{ele,ion}}{\partial t} + \nabla \mathbf{\Gamma}^{ele,ion} = S, \tag{1}$$

$$\nabla^2 \varphi = -\frac{e}{\varepsilon_0}(n^{ion} - n^{ele}), \tag{2}$$

where n is the number density of electrons and Ar^+ ions, $\mathbf{\Gamma}$ is the flux of particles, S is a source term, φ is a potential and ε_0 is the dielectric constant. The source term S is expressed by relation:

$$S = \alpha \Gamma^{ele} - \beta n^{ele} n^{ion}, \tag{3}$$

where α is Townsend ionization coefficient and β is the coefficient of recombination.

The extend fluid model, beside the continuity and Poisson's equations, has the electron energy balance equation:

$$\frac{\partial (n^{ele} u^{ele})}{\partial t} + \frac{5}{3} \nabla \mathbf{\Gamma}_u^{ele} = -e\mathbf{E} \cdot \mathbf{\Gamma}^{ele} - k_i u^{ion} n^{ele} N, \tag{4}$$

where u^{ele} is mean electron energy, $\mathbf{\Gamma}_u^{ele}$ is the electron energy flux, $\mathbf{E}$ is the electric field, k_i is ionization rate coefficient, $u^{ion} = 15.8\,eV$ is the ionization energy of argon atoms and N is number density of neutral gas.

The equations for fluid model with nonlocal ionization are the same as for the simple fluid model (1, 2). The ionization by fast electrons is included in this model and the source term has the form:

$$S_{fast}(x) = \begin{cases} \Gamma^{ele}(0)\alpha \exp(\alpha x) & \text{for } x < d_c \\ \Gamma^{ele}(0)\alpha \exp(\alpha d_c)\exp(-(x-d_c)/\lambda) & \text{for } x \geq d_c, \end{cases} \tag{5}$$

where $\Gamma^{ele}(0)$ is the electron flux at cathode, x is the distance from cathode, λ is the decay constant and d_C is the length of cathode sheath region where the electric field is strong. The ionization coefficient α used in equation 5 is a function of reduced field over the cathode sheath [21].The decay constant is calculated from the relation $\lambda = \varphi(d_c)/[(pC-d)(\alpha d_c)]$ [21], where $\varphi(d)$ is the cathode sheath voltage and C is the constant. The values of the transport and kinetic coefficients of electron and argon atom ion using for the modelling are taken from [19, 20, 22].

3. Experimental details

The measurements of static breakdown voltages, current-voltage characteristics and time delays are performed on gas tube presented in fig.1. The tube was evacuated down to 10^{-7} *Torr*, baked at 600*K*, and then filled with argon with an impurity level below 1 *ppm* (Matheson Co.) at pressure p =1.5*Torr*. The gas tube is made of borosilicate glass, with volume of $V \approx 60cm3$ and the plane-parallel cylindrical OFHC copper electrodes. The radius of electrodes is $R = 11mm$, while the inter-electrode distance d is variable.

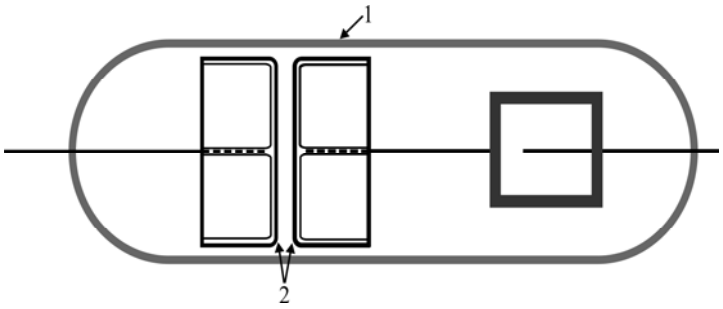

Figure 1. Schematic cross section of the discharge tube:
1- borosilicate glass and 2 – copper electrodes

4. Paschen curve modelling

The minimum voltage required for breakdown is the static breakdown voltage U_s. For the breakdown occurrence, the condition $\gamma(exp(\alpha d) - 1) \geq 1$ must be fulfilled , where γ is the secondary electron yield. The simple fluid model is applied for the calculation of static breakdown voltages and the results are compared to the experiment. The equations 1 and 2 are partial differential equation and for solving them finite difference method is used. After discretization, these equations in one and two dimension cases have the following form:

1D:

$$\frac{n_i^{k+1} - n_i^k}{\Delta t} + \frac{\Gamma_{i+1/2}^{k+1} - \Gamma_{i-1/2}^{k+1}}{\Delta x} = S_i^k, \tag{6}$$

$$\frac{\varphi_{i+1}^{k+1} - 2\varphi_i^{k+1} + \varphi_{i-1}^{k+1}}{\Delta x^2} = -\frac{\rho_i^k}{\varepsilon_0}, \tag{7}$$

2D:

$$\frac{n_{i\,j}^{k+1} - n_{i\,j}^k}{\Delta t} + \frac{1}{r_j}\frac{\Gamma_{i\,j+1/2}^{k+1} - \Gamma_{i\,j-1/2}^{k+1}}{\Delta r} + \frac{\Gamma_{i+1/2\,j}^{k+1} - \Gamma_{i-1/2\,j}^{k+1}}{\Delta z} = S_{i\,j}^k, \tag{8}$$

$$\frac{1}{r_j}\frac{\varphi_{i\,j+1}^{k+1} - 2\varphi_{i\,j}^{k+1}}{\Delta r} + \frac{\varphi_{i+1\,j}^{k+1} - 2\varphi_{i\,j}^{k+1} + \varphi_{i-1\,j}^{k+1}}{\Delta z^2} + \frac{\varphi_{i\,j+1}^{k+1} - 2\varphi_{i\,j}^{k+1} + \varphi_{i\,j-1}^{k+1}}{\Delta r^2} = -\frac{\rho_{ij}^k}{\varepsilon_0}, \tag{9}$$

where i and j are the spatial indices, k is the time index, ρ is the charge density , Δt is the time step and Δz and Δr are the spatial steps. Flux terms in equations 6 and 8 are expressed in exponential form introduce by Sharffeter and Gummel [23].The equations (6-9) present the system of linear equations and for solving them successive over relaxation method is used.

The values of electron transport coefficients and argon atom ion mobility are function of reduced field [19, 22], while the diffusion coefficient of argon atom ion is calculated from relation $D^{ion} = 200/p[cm^2 s^{-1}]$[19]. Based on the temporal evolution of Ar atom ion number density, the static breakdown voltage is determined. When the applied voltage U_w is equal to or greater than the static breakdown voltage U_s the number density of argon ion increases with increasing time (fig. 2).

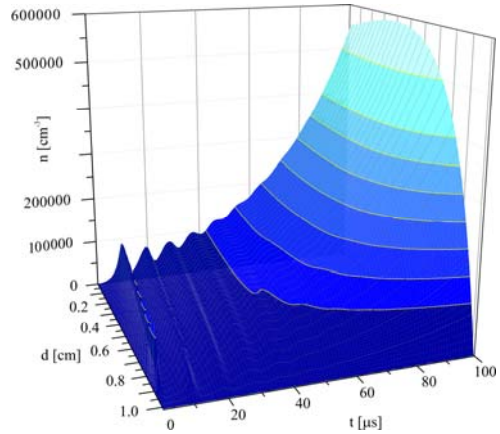

Figure 2. The temporal evolution of atomic argon ion when applied voltage is equal to or greater than the static breakdown voltage $U_w \geq U_s$ (U_s=214V)

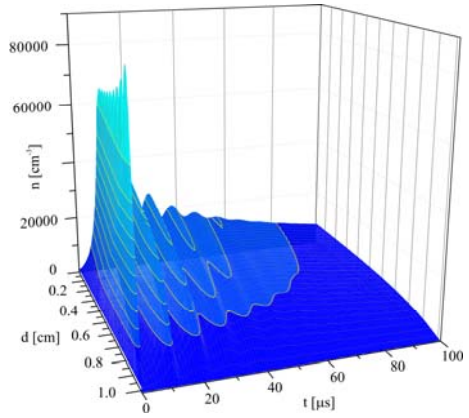

Figure 3. The temporal evolution of atomic argon ion when applied voltage is lower than the static breakdown voltage $U_w < U_s$ (U_s=214V)

In the cases when the applied voltage is lower than static breakdown voltage, the breakdown condition is not fulfilled and the number density of argon ion decreases with increasing time (fig.3). The modelling of Paschen curve is carried out for different values of secondary electron yield and the results are compared to the experimental data. The best agreement is achieved by using the variable secondary electron yield obtained from the breakdown condition for different values of *pd* (fig. 4a). The values for first Townsend ionization coefficient used for calculation of secondary electron yield is obtained by fitting the experimental data [24]. The agreement of secondary electron yield with data from literature [25] is given in fig. 4b.

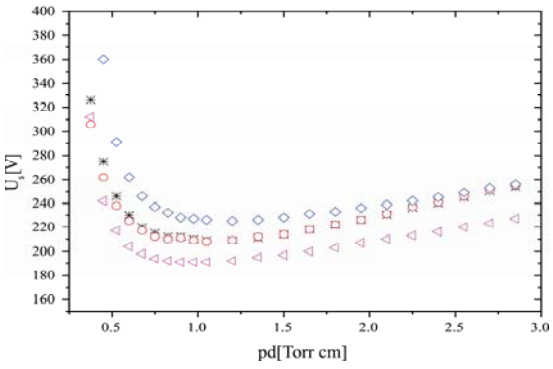

Figure 4a. Paschen curves obtained from experiment and models: ✳- experiment, ○-modelled with variable γ, ◁ -modelled with γ= 0.015, ◇-modelled with γ= 0.007

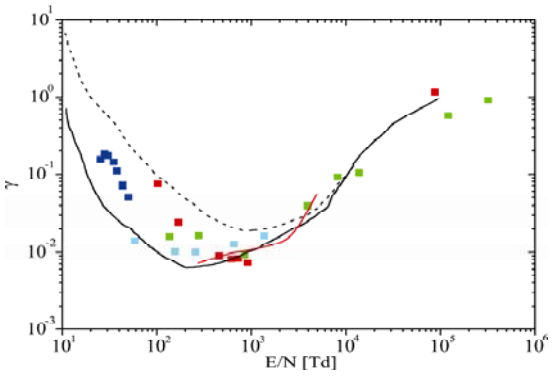

Figure 4b. Secondary electron yield in the function of reduced field *E/N*: red line is the secondary electron yield obtained from the breakdown condition and other symbols are from the paper [25]

5. The applicability of fluid models for modelling of current-voltage characteristics

The current-voltage (*I-U*) characteristics of the gas tube are measured for inter-electrode distances *d*=15*mm*, 12*mm* and 6*mm* (fig 5). In this paper the modelling of *I-U* characteristics is performed by using the one dimensional models. One dimensional models are applicable if all cathode area is occupied by glow, which is the case in the abnormal region of the glow discharge (100-600 μA), fig 5.

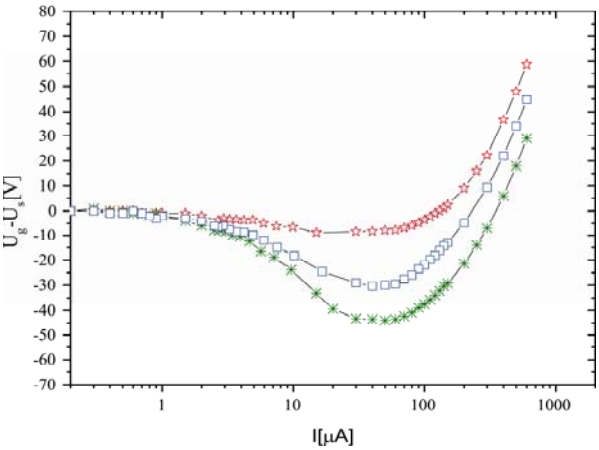

Figure 5. The (I-U) characteristics of glow discharge for different inter-electrode distances: ✳ - *d*=15*mm*, □ - *d*=12 *mm* and ☆- *d*=6 *mm*

The simple, extend and fluid models with nonlocal ionization are applied for *I-U* characteristics modelling and comparison of modelled and experimental data for inter-electrode distances *d*=15 *mm* and 12 *mm* are presented in fig.6. The values of secondary electron yield for these inter-electrode distances are γ=0.00809 and 0.00922, respectively. These values are obtained from the breakdown condition and used for the modelling as a simple approximation, but it should be noted that many authors have shown that secondary electron yield is not constant along I-U characteristics [26-28]. The best agreement with experiment is achieved by applying the fluid model with nonlocal ionization, while the results from other models deviate from experimental data.

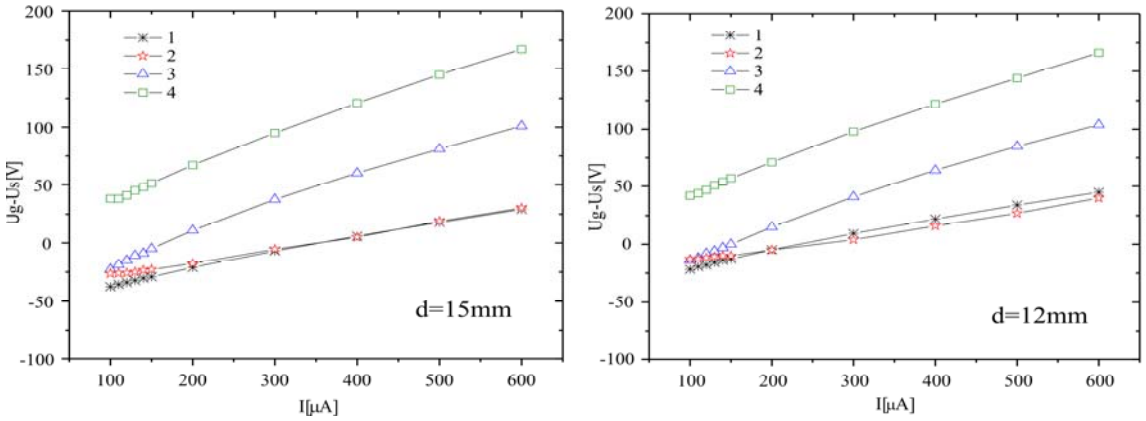

Figure 6. The current-voltage characteristics of abnormal glow discharge (100-600 μA) for the inter-electrode distances *d*=15*mm* and 12*mm* obtained from experiment and different models:
1- experiment, 2 - fluid model with nonlocal ionization, 3 - extend fluid model and 4 - simple fluid model

In the case when d =0.6cm, the region beyond the cathode space is very thick and the ionization by fast electrons in this region can be neglected, so the extend fluid model shows good agreement with the experiment (fig.7). However, the results from the simple fluid model still deviate from the experimental data. The value of secondary electron yield in this case is γ=0.00994.

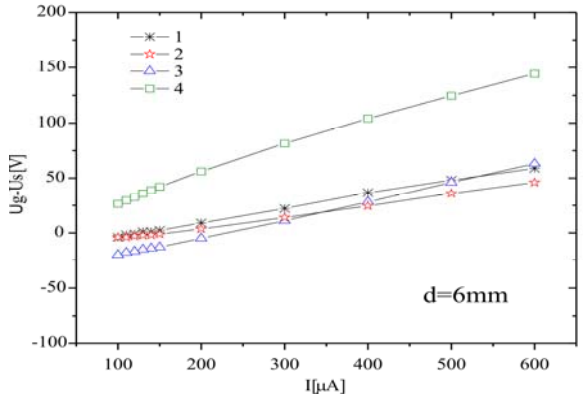

Figure 7. The current-voltage characteristics of abnormal glow discharge (100-600 μA) for the inter-electrode distance d=0.6 cm obtained experiment and different models: 1 - experiment, 2 - fluid model with nonlocal ionization, 3 - extend fluid model and 4 - simple fluid model

6. The comparison of measured and modelled formative time delays

The time that elapses from the moment of applying of voltage greater than the static breakdown voltage U_s to the breakdown occurrence, is denoted as the breakdown time delay t_d. It consists of statistical time delay t_s (from the application of voltage to the appearance of a free electron that initiates the breakdown) and the formative time delay t_f (from this moment to the collapse of the applied voltage and occurrence of a self-sustained current) [13, 14]. The time delay measurements were carried out by applying the step pulses (fig. 8) at different overvoltages $\Delta U = U_w - U_s$ and relaxation times (afterglow period) τ.

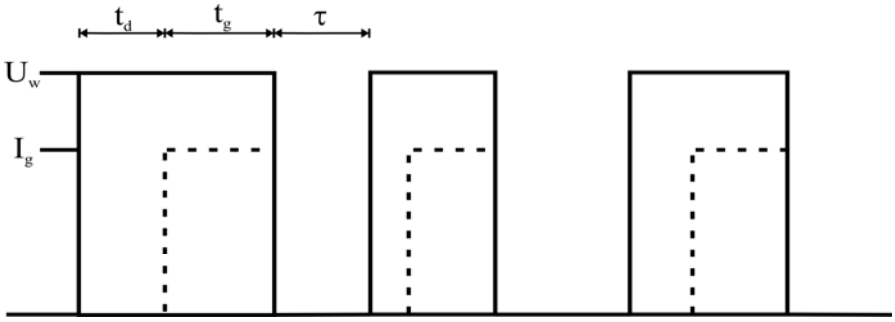

Figure 8. The sequence of pulses applied to the discharge tube: U_w - working voltage, I_g - glow current, t_d - breakdown time delay, t_g - glow time and τ- afterglow period.

The electron current density from the cathode is expressed by the relation [29, 30]:

$$i(t) \approx i_0 + qi(t - t_i) \approx i_0 + q[i(t) - t_i(di/dt)], \tag{10}$$

where i_0 is the current density of the seed electrons, $t_i = d/w_i$ is the ion transit time from anode to cathode and w_i is the ion drift velocity. After integration, the current density is obtained:

$$i(t) = i_0\left[\frac{q}{q-1}\exp\left(\frac{q-1}{q}\frac{t}{t_i}\right) - \frac{1}{q-1}\right], \tag{11}$$

and relation for formative time delay has the following [29, 30]:

$$t_f = \frac{q\,t_i}{q-1}\ln\frac{1+(q-1)(i/i_0)}{q}, \tag{12}$$

where q is the multiplication factor of electron avalanche. The multiplication factor is expressed by the relation:

$$q = \tilde{\gamma}\frac{\alpha}{\tilde{\alpha}}[\exp(\tilde{\alpha}\,d)-1], \tag{13}$$

where $\tilde{\alpha}$ is the electron ionization coefficient with included radial diffusion loss of electrons [31]:

$$\tilde{\alpha} = \alpha - (D_e / w_e)(2.4/R)^2. \tag{14}$$

The formative time dependence on overvoltage is presented in fig. 9.

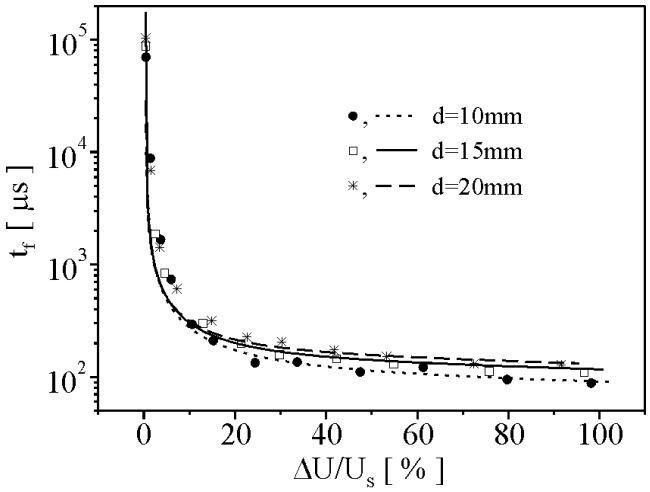

Figure 9. Formative time delays (●, □, ∗) and the corresponding line fits.

For the calculation of formative time delays 1D and 2D fluid models are also applied. In fig. 10 the comparison between modelled and measured formative time delay is presented. The formative time delay calculated from one dimensional fluid model is much shorter than measured ones because the radial diffusion of particles is not included in the model, while in case of two dimensional modelling, a very good agreement with experiment is achieved.

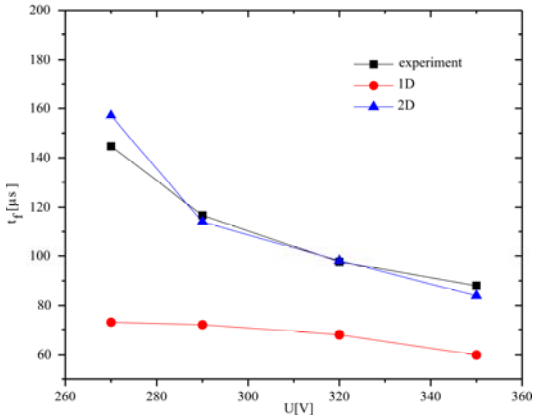

Figure 10. Comparison of formative time delay obtained from experiment and from fluid models.

7. The analysis of memory effect

The afterglow kinetics in argon is studied by the breakdown time delay measurements as a function of relaxation time $\overline{t_d}(\tau)$ (memory curve), fig. 11. The memory effect is the long time variation of the electrical breakdown time delay on the relaxation time (τ). The memory curve is divided in three regimes: in the first regime (early relaxation) the main process of breakdown initiation is secondary electron emission caused by ions, in the second regime (late relaxation) electrons are generated by surface recombination of nitrogen atoms present as impurities [15-17] and the third regime presents the saturation of memory curve caused by the cosmic rays and natural radioactivity.

The mean value of the statistical time delay can be expressed as:

$$\overline{t_S} = \frac{1}{YP}, \qquad Y = \gamma \cdot \Gamma \cdot S, \tag{15}$$

where Y represents a number of generated electrons in the inter-electrode space per second (electron yield), P is the probability of one electron to cause the breakdown [32, 15], γ is the coefficient for secondary electron yield, Γ is the flux of particles and S is the front area of cathode surface. More details about calculation of electron yield can be found in [16].

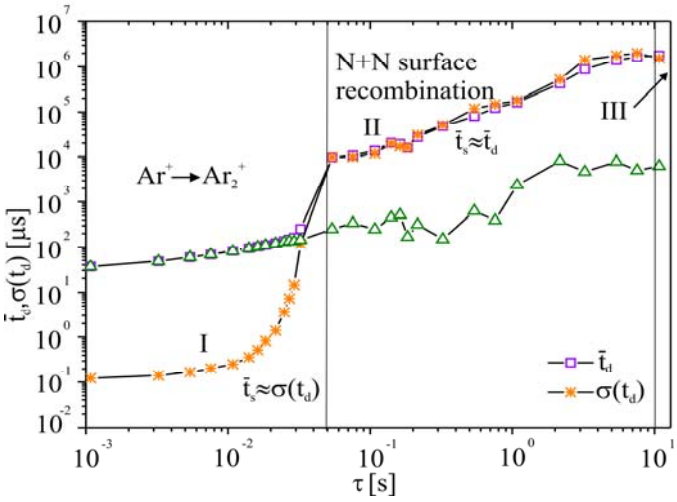

Figure 11. Argon memory curve t_d (τ) and time delay standard deviation $\sigma(t_d)$ for glow current *I=130mA*, working voltage *U=250V* and inter-electrode distance *d=10mm*

The number densities of Ar^+, Ar_2^+ ions and Ar^* ($^3P_2$) metastable state in afterglow is determined by solving the equation:

$$\frac{\partial n}{\partial \tau} - D \cdot \nabla^2 n = S, \tag{16}$$

where D is the diffusion coefficient of particles and S is the term in which the processes of production and loss of particles are included [15]. In the term S different reactions are included for which the rate coefficients are used from [16, 33, 34]. The temporal evolution of number density of nitrogen atoms, present as impurities, is obtained by the equation:

$$\frac{d[N]}{d\tau} = -\gamma_{nw}[N]^2, \tag{17}$$

where $[N]$ is the number density of nitrogen atom and γ_{nw} is the effective second order surface recombination coefficient on glass walls.

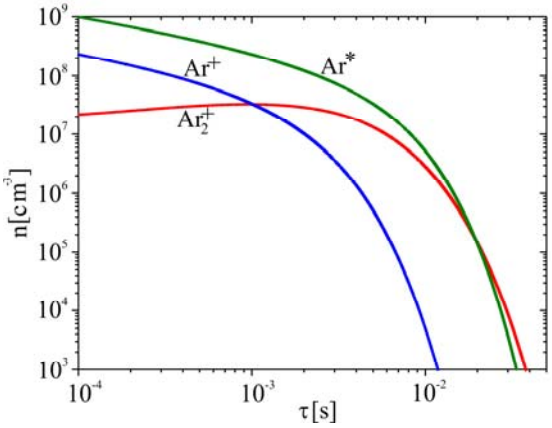

Figure 12. Number densities evolution of Ar^+ , Ar_2^+ ions and Ar^* ($^3P_2$) metastable state in afterglow

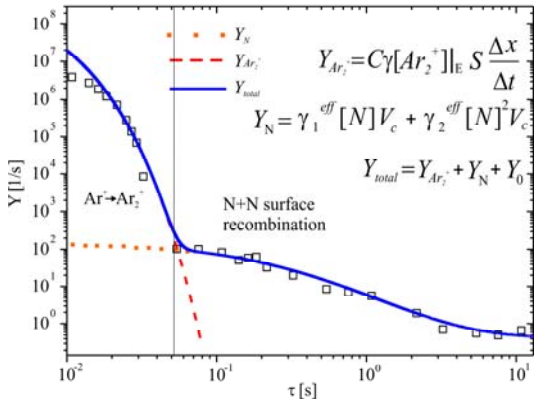

Figure 13. Fitting of the electron yield

In fig.12, the temporal evolution of Ar^+, Ar_2^+ ions and Ar^* ($^3P_2$) metastable state number densities are presented. It can be noticed that the number density of Ar^+ ion decreases due to the conversion of Ar^+ into Ar_2^+ (fig.12). In the fig. 13 the relations for electron yield cause by Ar_2^+ and nitrogen atoms are written [16], where C is the proportionality constant, γ is secondary electron yield cause by Ar_2^+ ion, $[Ar_2^+]\|_E$ is the molecular argon ion mean number density in the last grid points next to the front cathode surface, S is a front area of cathode surface, Δx is the grid spacing, Δt is the numerical time step, $[N]$ is the nitrogen atom number density, V_C is the inter-electrode space volume, Y_0 is the electron yield cause by the cosmic and background radiation and γ_1^{eff}, γ_2^{eff} are the effective gas phase rate coefficients for the surface recombination on the cathode and are first and second order, respectively. It is shown that only the decay of molecular argon ions Ar_2^+ can fit the experimental values for the electron yield and explain the early memory effect in argon (fig.13). For longer afterglow times, a very good fit of the electron yield is obtained by the surface recombination of nitrogen atoms present as impurities.

8. Conclusion

For the analysis of glow discharge many different numerical and analytical models were often applied. The Paschen curve is modelled and the best agreement with the experiment is achieved by using the fluid model with variable secondary electron yield. The current-voltage characteristics are measured for different inter-electrode distances and the fluid model with nonlocal ionization gives the best results for all inter-electrode distances. For formative time delays, the results from analytical model with included radial diffusion of electron and 2D fluid model are in a good agreement with the experiment. The memory effect is analyzed and it was found that the early afterglow kinetics is dominated by the decay of molecular argon ions and after that (for longer afterglow times) nitrogen atoms present as impurities are recombined on the cathode surface providing secondary electrons for breakdown initiation.

Acknowledgments

The author is grateful to the Ministry of Education, Science and Technological development of the Republic of Serbia (projects 171025).

References

[1] Lieberman M A and Lichtenberg A J 1994 *Principles of Plasma Discharges and Materials Processing* (New York : Jon Wiley & Sons)
[2] Papas D 2011 *J. Vac. Sci. Technol.* A **29** 020801
[3] Slusher R E 1999 *Rev. Mod. Phys.* **71** S471
[4] Zissis G and Kitsinelis S 2009 *J. Phys. D: Appl. Phys.* **42** 173001
[5] Chang J S, Wang H, Zhang Q G and Qui A 2011 *Plasma Sci. Technol.* **13** 719
[6] Neyts E C, Yusupov M, Verlackt C C and Bogaerts A 2014 *J. Phys. D: Appl. Phys.* **47** 293001
[7] Kong M G, Kroesen G, Morfill G, Nosenko T, Shimizu T, J. van Dijk and Zimmermann J L 2009 *New J.Phys.* **11** 115012
[8] Ward A L 1958 *Phys. Rev.* **112** 1852
[9] Davies A J, Davies C S and Evans C J 1971 *Proc. IEE* **118** 816
[10] Winkler R and Wilhelm J 1988 *Phys. Scr.* **T23** 264
[11] Stankov M N, Petković M D, Marković V LJ, Stamenković S N and Jovanović A P 2014 *Rom. J. Phys.* **59** 328
[12] Kulikovsky A A 1998 *Phys. Lett. A* **245** 445
[13] Bošan Dj A 1978 in *Proceedings of 5th International Conferenc on Gas Discharges* (Liverpool University, Liverpool UK) pp. 273–276
[14] Bošan Dj A and Pejović M M 1979 J. Phys. D **12**, 1699.
[15] Marković V Lj, Petrović Z Lj and Pejović M M 1994 *J. Chem. Phys.* **100** 8514
[16] Marković V Lj, Gocić S R, Stamenković S N and Petrović Z Lj 2005 *Phys. Plasmas* **12** 073502
[17] Huo W G, Jian S J, Yao J and Ding Z F 2014 *Phys. Plasmas* **21** 053505
[18] Fiala A, Pitchford L C and Boeuf J P 1994 *Phys. Rev. E* **49** 5607
[19] Rafatov I R, Akbar D and Bilikmen S 2007 *Phys. Lett. A* **367** 114
[20] Becker M M, Loffhagen D and Schmidt W 2009 *Comput. Phys. Commun.* **180** 1230
[21] Rafatov I, Bogdanov E A and Kudryavtsev A A 2012 *Phys. Plasmas* **19** 093503
[22] Hagelaar G J M and Pitchford L C 2005 *Plasma Sources Sci. Technol.* **14** 722, BOLSIG+ 2005 CPAT: http://www.bolsig.laplace.univ-tlse.fr/download.php
[23] Scharfetter D and Gumell H 1969 *IEEE Trans. electron devices* **16** 64
[24] Kruithof A A 1940 *Physica* **7** 519
[25] Phelps AV and Petrović Z Lj 1999 *Plasma Sources Sci. Technol.* **8** R21.
[26] Donko Z 2001 *Phys. Rev. E* **64** 026401
[27] Phelps A V 2001 *Plasma Source Sci. Tech.* **10** 329
[28] Marić D et al 2002 *Eur. Phys. J. D* **21** 73
[29] Raizer Y P 1991 *Gas Discharge Physics,* (Berlin: Springer)
[30] Marković V Lj, Stamenković S N and Gocić S R 2007 *Contrib. Plasma Phys.* **47** 413
[31] Marković V Lj, Stamenković S N, Gocić S R, Jovanović A P and Stankov M N 2012 in *Proceedings of the 26th Summer School and Int. Symp.on the Physics of Ionized Gases*, editors M. Kuraica and Z. Mijatović (Zrenjanin, Serbia) p. 253
[32] Morgan C G 1978 in *Electrical Breakdown of Gases*, edited by Meek J M and Craggs J D John (Chichester: Wiley & Sons)
[33] Bogaerts A and Gijbels R 1999 *J. Appl. Phys.* **86** 4124
[34] Li Z, Zhao Z and Li X 2012 *Phys. Plasmas* **19** 033510